Journal of Applied Pharmaceutical Science Vol. 13(11), pp 170-177, November, 2023
Available online at http://www.japsonline.com
DOI: 10.7324/JAPS.2023.140149
ISSN 2231-3354

Synthesis, *Mycobacterium tuberculosis* $H_{37}Rv$ inhibitory activity, and molecular docking study of pyrazinamide analogs

Muhammad Zulqurnain[1], Nur Pasca Aijijiyah[1], First A. Wati[1], Arif Fadlan[1], Azminah Azminah[2], Mardi Santoso[1*]

[1]Department of Chemistry, Faculty of Science and Analytical Data, Institut Teknologi Sepuluh Nopember, Surabaya, Indonesia.
[2]Faculty of Pharmacy, University of Surabaya, Surabaya, Indonesia.

ARTICLE INFO

Received on: 17/05/2023
Accepted on: 20/09/2023
Available Online: 04/11/2023

Key words:
Pyrazine-2-carboxamides, yamaguchi reaction, 2,4,6-trichlorobenzoyl chloride, antitubercular activity, molecular docking.

ABSTRACT

Pyrazinamide analogs **5a–h** have been successfully synthesized by the Yamaguchi esterification method with yields ranging from 6% to 86%. Among pyrazinamides **5a–h**, pyrazinamides **5d**,**g** showed the best antituberculosis activity with MIC values <6.25 µg/ml. Based on the molecular docking studies, all the synthesized pyrazinamide had lower binding energy than pyrazinamide itself (−5.21 kcal/mol), except **5e** with a value of −2.83 kcal/mol. Pyrazinamides **5d** and **5g** showed lower binding energy (−6.36 and −5.91 kcal/mol, respectively) than the native ligand (−5.83 kcal/mol) and pyrazinamide (−5.21 kcal/mol). The lower binding energy of **5d** than that of **5g** because it interacted strongly with Arg54* via hydrogen bonding, while **5g** only interacted via π-cation interaction. However, **5g** formed two hydrogen bonds with Tyr90* and Thr57 residues. These findings suggest that the most active compounds **5d**, **g** could be regarded as promising candidates for discovering new antitubercular drugs.

INTRODUCTION

Tuberculosis (TB) is an airborne infectious disease that attacks the lungs. The disease is caused by the bacillus *Mycobacterium tuberculosis* and has become one of the top 10 leading causes of death in the world (Adigun and Singh, 2022; Bhargava and Bhargava, 2020). According to the World Health Organization, in 2019, an estimated 10 million people suffered from TB, of which 206,030 people suffered from multidrug-resistant TB (MDR-TB) and about 1.2 million of these people died (Calnan *et al*., 2022). In addition, the emergence of drug-resistant TB can hinder TB treatment. Resistance to TB drugs can be MDR-TB involving resistance to first-line drugs such as isoniazid, rifampicin, and pyrazinamide, and extensive drug-resistant TB involving resistance to fluoroquinolones and second-line injectable drugs. Resistance to TB drugs is caused by inappropriate and nonadherent patients in treatment (Alexander and De, 2007; Seung *et al*., 2015; Teixeira *et al*., 2020). COVID-19 is an infectious disease similar to TB, which attacks the lungs with symptoms such as cough, fever, and shortness of breath, which is currently a worldwide pandemic (Selvina, 2020). TB patients with COVID-19 suffer from severe pulmonary fibrosis (Tamuzi *et al*., 2020). TB drug resistance in combination with COVID-19 infections has prompted the development of new antituberculosis drugs that are less resistant, more active, and more effective.

Standard TB treatment is carried out by taking first-line drugs, namely, pyrazinamide, isoniazid, rifampicin, and ethambutol for 2 months, followed by taking isoniazid and rifampicin for 4 months (Abdel-Aziz and Abdel-Rahman, 2010; Sotgiu *et al*., 2015). Pyrazinamide is a drug with a strong inhibitory effect on *M. tuberculosis* and is an important factor in shortening TB treatment from 9–12 to 6 months. Pyrazinamide can kill the semidormant *M. tuberculosis* population in an acidic pH environment, which is not killed by other TB drugs (Zhang, 2004; Zhang *et al*., 2003). Based

*Corresponding Author
Mardi Santoso, Department of Chemistry, Faculty of Science and Analytical Data, Institut Teknologi Sepuluh Nopember, Surabaya, Indonesia.
E-mail: tsv09 @ chem.its.ac.id

on these advantages, pyrazinamide analogs need to be developed. Pyrazinamide analogs substituted with 6-chloro on the pyrazine ring exhibit good activity (Dolezal *et al*., 2009, 2008; Servusová *et al*., 2012; Zitko *et al*., 2016). Substitution on the N atom of the pyrazinamide with ethylphenyl, cycloheptyl, octyl, adamantyl, and 4-chlorobenzyl has been accomplished by a general method involving thionyl chloride, and the analogs showed better activity against *M. tuberculosis* (Onajole *et al*., 2013; Pieroni *et al*., 2011; Semelkova *et al*., 2015; Zitko *et al*., 2013). Thionyl chloride is included in the list of the Chemical Weapons Convention, so it is very difficult to import in various countries, especially in Indonesia (Kuitunen *et al*., 2020; Wirth, 2001). Synthesis of the pyrazinamide analogs was also carried out using 1,1'-carbonyldiimidazole (CDI) reagent as a substitute for thionyl chloride. However, CDI is less reactive than thionyl chloride and is easily hydrolyzed in the presence of water (Bouz *et al*., 2019).

This study reports on the synthesis of pyrazinamide analogs using the Yamaguchi esterification reaction method and reports on their antituberculosis activity (Kamadatu and Santoso, 2016). It also reports on the docking studies of these compounds in the active site of *M. tuberculosis* protein.

MATERIALS AND METHODS

General

All chemicals used were purchased from Sigma-Aldrich, Tokyo Chemical Industry, and Merck and were used without further purification. The solvents used for elutions in column chromatography and chromatotron are distilled before use. Melting point analysis was carried out on a Fisher–Johns melting point apparatus and is uncorrected. The infrared spectrum was obtained using FT-IR Shimadzu 8400s measured in KBr solids. Jeol Resonance nuclear magnetic resonance (NMR) Spectrometer (400 MHz for ^{1}H NMR and 100 MHz for ^{13}C NMR) was used to obtain NMR spectra with tetrametilsilan as standard analyzed in deuterated chloroform solvent. High-resolution mass spectra (HRMS) were obtained from the Waters Q-TOF Xevo instrument.

General procedure for the synthesis of pyrazinamide analogs (5a–h)

A solution of pyrazine-2-carboxylic acid or 6-chloropyrazine-2-carboxylic acid (1 eq) in THF (200 ml) was added to a mixture of 2,4,6-trichlorobenzoyl chloride (1 eq) and triethylamine (TEA) (1 eq). The reaction mixture was stirred at room temperature for 20 minutes, followed by the addition of dimethylaminopyridine (DMAP) (1 eq) and aniline or amine (0.25 eq). The mixture was then heated at reflux at 66°C/55°C for 1 hour. After the reaction (TLC) was completed, the mixture was cooled, filtered, diluted with distilled water, and then extracted with dichloromethane (2 × 25 ml). The organic phase was washed successively with 5% hydrochloric acid (25 ml), 5% NaOH (25 ml), 5% $NaHCO_3$ (25 ml), and distilled water (25 ml) and then dried over anhydrous magnesium sulfate. The solvent was removed under reduced pressure to give off-white solids. Compounds **5a**, **c**, **d**, **e** were purified using chromatotron or column chromatography (ethyl acetate: *n*-hexane), while compound **5b** was obtained in a pure state without purification.

***N-(4-ethylphenyl)pyrazine-2-carboxamide* (5a)**

White solid; yield = 50%; mp = 133°C–134°C; IR (KBr) υ_{max} 3,345 (N-H), 3,088 (C-H aromatic), 2,960 and 2,928 (C-H aliphatic), 1,678 (C=O), 1,522 (C=N) cm^{-1}. ^{1}H NMR (400 MHz, $CDCl_3$) δ 9.62 (bs, 1H, NH), 9.49 (d, J = 1.4 Hz, 1H, ArH), 8.77 (d, J = 2.4 Hz, 1H, ArH), 8.56 (dd, J = 2.4, 1.5 Hz, 1H, ArH), 7.65 (d, J = 8.4 Hz, 2H, ArH), 7.22 (d, J = 8.4 Hz, 2H, ArH), 2.63 (q, J = 7.6 Hz, 2H, CH_2), 1.22 (t, J = 7.6 Hz, 3H, CH_3).$^{-13}$C NMR (100 MHz, $CDCl_3$) δ 160.6, 147.5, 144.7, 144.6, 142.5, 141.1, 134.9, 128.6, 120.0, 28.5, 15.8. HRESIMS *m/z* (pos): 228.1135 $C_{13}H_{13}N_3O$ (calcd. 228.1137).

***N-cycloheptylpyrazine-2-carboxamide* (5b)**

Yellow solid; yield = 86%; mp = 105°C–106°C; IR (KBr) υ_{max} 3,358 (N-H), 3,090 (C-H aromatic), 2,926 and 2,857 (C-H aliphatic), 1,659 (C=O), 1,528 (C=N) cm^{-1}. ^{1}H NMR (400 MHz, $CDCl_3$) δ 9.37 (d, J = 1.3 Hz, 1H, ArH), 8.70 (d, J = 2.5 Hz, 1H, ArH), 8.48 (dd, J = 2.4, 0.9 Hz, 1H, ArH), 7.75 (bs, 1H, NH), 4.10–4.15 (m, 1H, CH), 2.01–1.98 and 1.67–1.53 (m, 12H, CH_2). ^{13}C NMR (100 MHz, $CDCl_3$) δ 161.7, 147.1, 144.9, 144.5, 142.5, 50.5, 35.1, 28.1, 24.1. HRESIMS *m/z* (pos): 220.1461 $C_{12}H_{17}N_3O$ (calcd. 220.1450).

***N-octylpyrazine-2-carboxamide* (5c)**

White solid; yield = 6%; mp = 57°C–58°C; IR (KBr) υ_{max} 3,310 (N-H), 3,055 (C-H aromatic), 2,955 and 2,918 (C-H aliphatic), 1,661 (C=O), 1,535 (C=N) cm^{-1}. ^{1}H NMR (400 MHz, $CDCl_3$) δ 9.39 (d, J = 1.2 Hz, 1H, ArH), 8.72 (d, J = 2.4 Hz, 1H, ArH), 8.50 (dd, J = 2.2, 1.4 Hz, 1H, ArH), 7.80 (bs, 1H, NH), 3.46 (q, J = 6.8 Hz, 2H, CH_2), 1.40–1.24 and 1.65–1.58 (m, 12H, CH_2), 0.85 (t, J = 6.8 Hz, 3H, CH_3). ^{13}C NMR (100 MHz, $CDCl_3$) δ 162.9, 147.2, 144.7, 144.5, 142.6, 39.6, 31.9, 29.8, 29.6, 29.3, 29.3, 27.1, 22.7, 14.2. HRESIMS *m/z* (pos): 236.1762 $C_{13}H_{21}N_3O$ (calcd. 236.1763).

***N-(4-chlorobenzyl)pyrazine-2-carboxamide* (5d)**

White solid; yield = 14%; mp = 134°C–135°C; IR (KBr) υ_{max} 3,364 (N-H), 3,102 (C-H aromatic), 2,957 and 2,922 (C-H aliphatic), 1,661 (C=O), 1,530 (C=N) cm^{-1}. ^{1}H NMR (400 MHz, $CDCl_3$) δ 9.43 (d, J = 1.3 Hz, 1H, ArH), 8.75 (d, J = 2.4 Hz, 1H, ArH), 8.51 (t, J = 1.8 Hz, 1H, ArH), 8.12 (bs, 1H, NH), 7.33–7.27 (m, 4H, ArH), 4.64 (d, J = 6.2 Hz, 2H, CH_2).$^{-13}$C NMR (100 MHz, $CDCl_3$) δ 163.1, 147.5, 144.6, 144.3, 142.7, 136.4, 133.6, 129.3, 129.0, 42.9. HRESIMS *m/z* (pos): 250.0650 $C_{12}H_{11}N_3O^{37}Cl$ (calcd. 250.0556) and 248.0592 $C_{12}H_{11}N_3O^{35}Cl$ (calcd. 248.0591).

***N-(adamantan-1-yl)pyrazine-2-carboxamide* (5e)**

Yellow solid; yield = 14 %; mp = 133°C–134°C; IR (KBr) υ_{max} 3,308 (N-H), 3,100 (C-H aromatic), 2,909 and 2,895 (C-H aliphatic), 1,662 (C=O), 1,524 (C=N) cm^{-1}. ^{1}H NMR (400 MHz, $CDCl_3$) δ 9.35 (d, J = 1.1 Hz, 1H, ArH), 8.67 (d, J = 2.5 Hz, 1H, ArH), 8.46 (dd, J = 2.4, 1.5 Hz, 1H, ArH), 7.58 (bs, 1H, NH), 2.12 (s, 9H, CH and CH_2), 1.70 (s, 6H, CH_2). ^{13}C NMR (100 MHz, $CDCl_3$) δ 161.8, 146.8, 145.5, 144.1, 142.3, 52.1, 41.5, 36.4, 29.5. HRESIMS *m/z* (pos): 258.1604 $C_{12}H_{17}N_3O$ (calcd. 258.1606).

6-Chloro-N-(4-ethylphenyl)pyrazine-2-carboxamide **(5f)**

Brownish orange solid; yield = 75%; mp = 103°C–104°C; IR (KBr) υ_{max} 3,370 (N-H), 3,044 (C-H aromatic), 2,959 and 2,916 (C-H aliphatic), 1,694 (C=O), 1,535 (C=N) cm^{-1}. ^1H NMR (400 MHz, $CDCl_3$) δ 9.39 (s, 1H, ArH), 9.35 (bs, 1H, NH), 8.79 (s, 1H, ArH), 7.65 (d, J = 8.8 Hz, 2H, ArH), 7.23 (d, J = 8.8 Hz, 2H, ArH), 2.65 (q, J = 8.0 Hz, 2H, CH_2), 1.24 (t, J = 8.0 Hz, 3H, CH_3). ^{13}C NMR (100 MHz, $CDCl_3$) δ 159.3, 147.5, 144.2, 142.3, 141.5, 138.8, 134.6, 128.6, 120.2, 28.5, 15.7. HRESIMS *m/z* (pos): 264.0656 $C_{13}H_{13}N_3O^{37}Cl$ (calcd. 264.0718) and 262.0606 $C_{13}H_{13}N_3O^{35}Cl$ (calcd. 262.0747).

6-Chloro-N-cycloheptylpyrazine-2-carboxamide **(5g)**

White solid; yield = 71%; mp = 47°C–48°C; IR (KBr) υ_{max} 3,273 (N-H), 3,065 (C-H aromatic), 2,920 and 2,857 (C-H aliphatic), 1,653 (C=O), 1,530 (C=N) cm^{-1}. ^1H NMR (400 MHz, $CDCl_3$) δ 9.28 (s, 1H, ArH), 8.73 (s, 1H, ArH), 7.56 (bs, 1H, NH), 4.17–4.11 (m, 1H, CH), 2.05–2.00 (m, 2H, CH_2), 1.71–1.55 (m, 10H, CH_2). ^{13}C NMR (100 MHz, $CDCl_3$) δ 160.5, 147.5, 147.1, 144.5, 142.1, 50.9, 35.1, 28.1, 24.2. HRESIMS *m/z* (pos): 256.0997 $C_{12}H_{17}N_3O^{37}Cl$ (calcd. 256.1031) and 254.0967 $C_{12}H_{17}N_3O^{35}Cl$ (calcd. 254.1060).

6-Chloro-N-octylpyrazine-2-carboxamide **(5h)**

White solid; yield = 73%; mp = 48°C–49°C; IR (KBr) υ_{max} 3,329 (N-H), 3,090 (C-H aromatic), 2,945 and 2,916 (C-H aliphatic), 1,670 (C=O), 1,530 (C=N) cm^{-1}. ^1H NMR (400 MHz, $CDCl_3$) δ 9.28 (s, 1H, ArH), 8.73 (s, 1H, ArH), 7.62 (bs, 1H, NH), 3.46 (q, J = 6.8 Hz, 2H, CH_2), 1.63 (p, J = 7.5 Hz, 2H, CH_2), 1.37–1.23 (m, 10H, CH_2), 0.86 (t, J = 8.0 Hz, 3H, CH_3). ^{13}C NMR (100 MHz, $CDCl_3$) δ 161.7, 147.6, 147.2, 144.2, 142.1, 39.8, 31.9, 29.6, 29.3, 29.3, 27.0, 22.7, 14.2. HRESIMS *m/z* (pos): 272.1357 $C_{13}H_{21}N_3O^{37}Cl$ (calcd. 272.1344) and 270.1252 $C_{13}H_{21}N_3O^{35}Cl$ (calcd. 270.1373).

Antitubercular activity

The resazurin microtiter method (REMA) was used to determine the minimum concentration of the pyrazinamide analogs (**5a–h**) that could inhibit the growth of *M. tuberculosis*. Each compound (**5a–h**) was dissolved in 20% dimethyl sulfoxide solution in water to obtain a stock solution with a final concentration of 1,000 ppm, which was then diluted to obtain a test solution with a concentration of 25, 12.5, 6.25, 3.13, 1.56, and 0.78 g/ml. The test solutions were then placed on a 96-well microplate. As much as 100 µl of *M. tuberculosis* $H_{37}Rv$ suspension was added to each well, with several wells serving as the positive control, media control, solvent control, compound control, and comparison compound (rifampicin). The microplate was then closed and sealed with a plastic bag and incubated at 37°C for 7 days. After that, 30 µl of resazurin 0.01% solution was added to each well and incubated at 37°C for 1 day. A color change is then observed (a color change from blue to pink indicates bacterial growth). The test was carried out in triplicate for each compound and each concentration.

Molecular docking study

The crystal structure of *M. tuberculosis* PanD protein (*Mtb*PanD) complexed with 6-chloro-pyrazinoic acid (NMJ) was downloaded from the Protein Data Bank (PDB ID: 6P02) (Sun *et al*., 2020). The receptor was prepared by removing all water molecules, adding polar hydrogens, and adding Kollman charge using the AutoDockTools package. The 2D structure of the ligands (**5a–h**) was drawn using MarvinSketch version 20.18. The MMFF94 (Merck Molecular Force Field) from MarvinSketch was then used to minimize the energy of each ligand (Gentile *et al*., 2020). The docking simulation was carried out using AutoDock 4.2.6 software (The Scripps Research Institute, La Jolla, CA, USA) (Santoso *et al*., 2022). The active site of the *Mtb*PanD was determined using a grid box centered on × : 47.435, *y*: −44.96, and z: 0.783 with an *xyz* dimension size of 22 × 28 × 22 and spacing of 0.375 Å. The Lamarckian genetic algorithm was used to search for the best ligand binding pose with a GA run of 100 (Harini *et al*., 2021). The docking results were analyzed using BIOVIA Discovery Studio Visualizer copyright © 2019 (Dassault Systèmes Biovia Corp, VélizyVillacoublay, France) (Yadav *et al*., 2017).

RESULTS AND DISCUSSION

Chemistry

Eight pyrazinamide analogs (**5a–h**) have been successfully synthesized by the Yamaguchi esterification reaction, as shown in Table 1 (Kamadatu and Santoso, 2016; Maharani and Santoso, 2015). The reaction is initiated by the deprotonation of the pyrazine-2-carboxylic acid (**1a**) or 6-chloro-pyrazine-2-carboxylic acid (**1b**) using to form triethylammonium carboxylate salt. The carboxylate anion then reacts with the carbonyl group of 2,4,6-trichlorobenzoyl chloride (**2**) via a nucleophilic substitution mechanism to form an asymmetric acid anhydride (**3**), which then reacts with 4- DMAP via a substitution mechanism to form a DMAP-substituted acyl. The amine or aniline then reacts with the DMAP-substituted acyl via a nucleophilic substitution mechanism to give the pyrazinamide analogs (**5a–h**) (Dhimitruka and SantaLucia, 2006). The yield of the pyrazinamide analogs (**5a–h**) ranged from 6% to 86%, and the structure of the target compounds was confirmed by IR, HRMS, and NMR.

Antitubercular activity

Pyrazinamide analogs (**5a–h**) were tested for bacterial growth inhibition activity against *M. tuberculosis* strain $H_{37}Rv$ using the resazurin microtiter REMA test (Annuur *et al*., 2018). The results of the bioactivity test were expressed as minimum inhibition concentration (MIC), which was the minimum concentration of the test compound capable of inhibiting bacterial growth, as seen in Table 2. Based on the Global Program for discovering new TB drugs, active compounds must have a MIC value below 6.25 µg/ml (Boechat *et al*., 2011). Pyrazinamides **5d**, **g** showed the best inhibition activity among the compounds tested with a MIC value of <6.25 µg/ml and had better activity than pyrazinamide itself (MIC = 100 µg/ml). Pyrazinamide **5f** had moderate activity with a MIC value of <12.5 µg/ml, which is still better than pyrazinamide. Meanwhile, pyrazinamides **5a–c**, **e**, **h** did not inhibit the growth of *M. tuberculosis* at each test concentration, resulting in a MIC value of >25 µg/ml.

The substitution of 4-chlorobenzyl (**5d**) on the amide group of pyrazinamide resulted in the strongest antituberculosis activity among analog compounds without Cl substitution on the

Table 1. Synthesis of pyrazinamides **5a–h**.

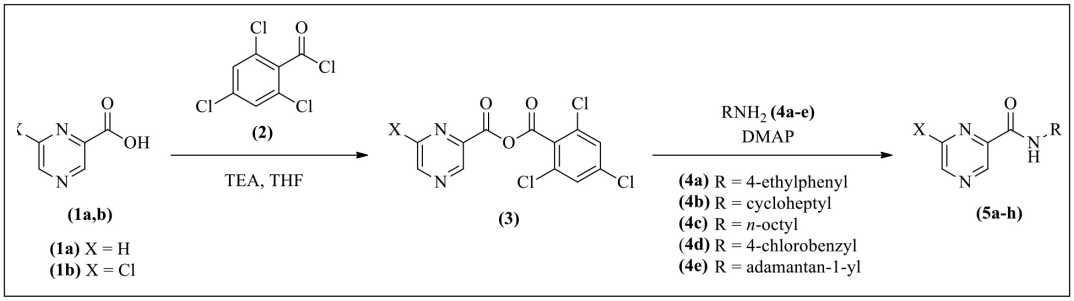

Entry	R	R_1	Pyrazinamides	Isolated Yield (%)
1	**1a**	**4a**	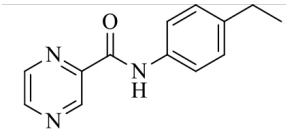 (**5a**)	50
2	**1a**	**4b**	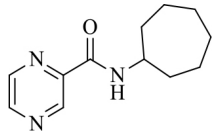 (**5b**)	86
3	**1a**	**4c**	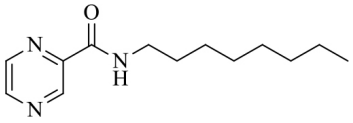 (**5c**)	6
4	**1a**	**4d**	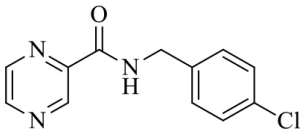 (**5d**)	14
5	**1a**	**4e**	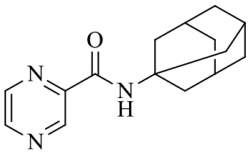 (**5e**)	14
6	**1b**	**4a**	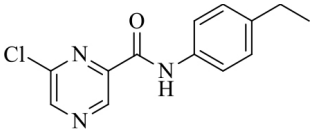 (**5f**)	75
7	**1b**	**4b**	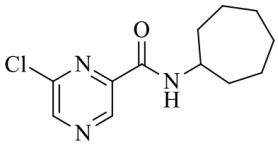 (**5g**)	71
8	**1b**	**4c**	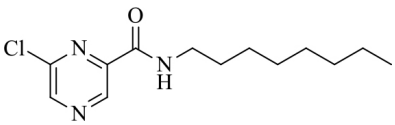 (**5h**)	73

Table 2. Test results of pyrazinamides **5a–h** activity against *M. tuberculosis* $H_{37}Rv$.

Compounds	MIC (µg/ml)	MIC (µM)
5a	>25	>0.11
5b	>25	>0.11
5c	>25	>0.11
5d	<6.25	<0.03
5e	>25	>0.10
5f	<12.5	<0.05
5g	<6.25	<0.03
5h	>25	>0.09
Rifampicin	0.25	0.003
Pyrazinamide (Campanerut *et al*., 2011)	100	0.81

pyrazine ring. The presence of the Cl atom at position-4 of the benzene ring and the extension of the amide bridge with $–CH_2$- could increase the inhibition of *M. tuberculosis* growth, while the presence of *para*-ethyl without $–CH_2$- moiety on **5a** gave a lower inhibition activity. Its activity is the same as that of the alkyl-substituted compounds (**5b, c, e**). The presence of Cl in position-6 of the pyrazine ring increased the *M. tuberculosis* inhibition activity. The inhibition activity of **5f** and **5g** was 2-fold and 4-fold, respectively, more potent compared to that of **5a** and **5b**. However, the activity of **5h** was still the same as that of **5c**.

Molecular docking study

PanD is an aspartate decarboxylase that converts L-aspartate to β-alanine in the pantothenate biosynthetic pathway. β-Alanine is necessary for the formation of vitamin B5 and coenzyme A in *M. tuberculosis* (Sun *et al*., 2020). CoA plays an important role in the biosynthesis and catabolism of lipids, which supplies the bacillus with its main source of energy during infection (Evans *et al*., 2016). In the pyrazinamide mode of action, PanD has been suggested as one of its target proteins. Pyrazinamide is a prodrug converted to its active form, pyrazinoic acid (POA), by the enzyme PncA. POA is thought to influence PanD activity in several postulated actions (Butman *et al*., 2020; Gopal *et al*., 2020). The molecular docking study was used to investigate the atomic behavior of the pyrazinamides **5a–h** at the active site of the *Mtb*PanD located at the junction of two neighboring subunits (PDB ID: 6P02), as can be seen in Figure 1A (Hassan *et al*., 2020). Before docking the target compounds (**5a–h**) to the *Mtb*PanD active site, the docking protocol was validated by redocking the native ligands (NMJ) at the *Mtb*PanD active site. The redocking process was considered successful if the root-mean-square deviation (RMSD) was less than 2 Å, indicating that the protocol used can reproduce the original ligand-target interaction (Morris *et al*., 2009). An RMSD value of 0.43 Å was obtained from the redocking of NMJ at the *Mtb*PanD active site at the junction of subunits 1 and 2, where the difference between crystallographic and redocked NMJ conformations is shown in Figure 1B.

Based on the results, the redocked NMJ produced a binding energy value of −5.83 kcal/mol and had almost the same interaction as the crystallographic NMJ, as shown in Figure 2. The

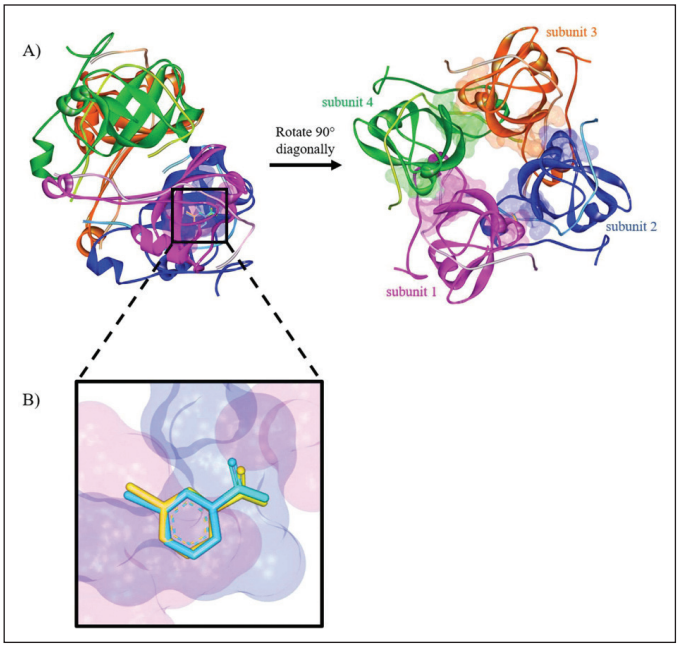

Figure 1. (A) The active sites of *Mtb*PanD tetramer are located at the junction of two neighboring subunits (PDB ID: 6P02), which are displayed by residue surfaces in various colors depending on the subunits. (B) The crystallographic NMJ conformation (cyan) is superimposed with the redocked NMJ conformation (yellow) in the active site of *Mtb*PanD at the junction of subunits 1 (magenta) and 2 (blue).

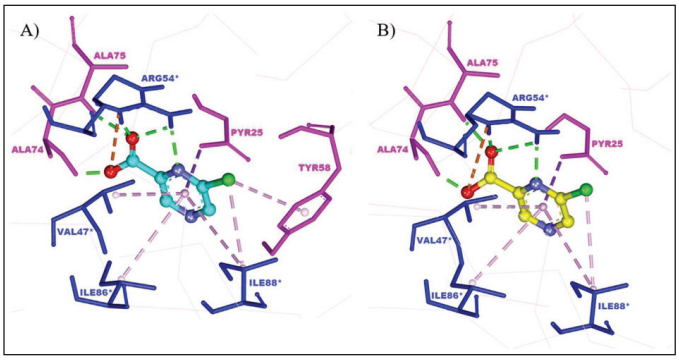

Figure 2. The binding mode of (A) crystallographic NMJ and (B) redocked NMJ at the *Mtb*PanD active site between subunits 1 and 2 (PDB ID: 6P02). The residues of subunits 1 and 2 are displayed in magenta and blue, respectively.

redocked NMJ formed four hydrogen bonds with three *Mtb*PanD key residues, namely, Ala74, Ala 75, and Arg54* (Sun *et al*., 2020). The N1 atom of the pyrazine ring is bound to Arg45*, the deprotonated carboxylate is bound to Ala74, and the oxygen atom of the carbonyl group (CO) group is bound to both Ala75 and Arg45*. Besides, the positive charge of the protonated amine at Arg54* attracted the negative charge of the deprotonated carboxylate at the redocked NMJ, resulting in a noncovalent interaction called an attractive charge. In addition, the 6-chlorine pyrazine ring formed several hydrophobic interactions, namely, π-σ interaction with Pyr25, alkyl interaction with Ile88*, and π-alkyl interactions with Val47*, Ile86*, and Ile88* residues. The sole difference between the crystallographic and redocked NMJ conformations was the type of contact made with the Tyr58 residue. The crystallographic NMJ

interacted with Tyr58 via π-alkyl interaction, whereas redocked NMJ interacted with this residue via van der Waals interaction.

Based on the redocking results, the docking protocol can be applied to simulate the docking of pyrazinamides **5a–h** to the *Mtb*PanD active site. Table 3 shows the binding energies and interacting residues of the pyrazinamides **5a–h** obtained from their docking simulation. According to the docking results, almost all the pyrazinamides **5a–h** have lower binding energies than the pyrazinamide itself (−5.21 kcal/mol). except **5e** with a value of -2.83 kcal/mol. The large binding energy value is possible because **5e** did not interact with the *Mtb*PanD key residue except for van der Waals interaction, which is a relatively weaker electric attraction than covalent bond and electrostatic interaction (Bronowska, 2011; Tallei *et al*., 2021). The two most active pyrazinamides **5d**, **g** have lower binding energy than both pyrazinamide (-5.21 kcal/mol) and NMJ (−5.83 kcal/mol). As seen in Figure 3, due to the presence of the amide bridge in the structure of **5d**, **g**, the aromatic cores of **5d**, **g** entered different spaces from the pyrazine core of NMJ at the *Mtb*PanD active site. The amide bridge of **5d**, **g** was in the same space as the pyrazine core of NMJ, whereas the pyrazine core of these two compounds was in the space following the tunnel where the Cl atom of NMJ is located. The 4-chlorobenzyl and cycloheptyl moieties of **5d** and **5g**, respectively, entered the cavity adjacent to where the carboxylate group of NMJ is located.

The oxygen atom of the CO in **5d** formed two hydrogen bonds with key residue Arg54* (Fig. 4A). Both pyrazine core and 4-chlorobenzyl moiety of **5d** are bound to the hydrophobic cavity residues. The pyrazine core formed π-σ and π-alkyl interactions with Ile88* and Val47*, respectively. The benzene core of 4-chlorobenzyl moiety formed π-π T-shaped interaction with His11* and π-σ interactions with Ile86* and Pyr25 residues, whereas its Cl atom is bound to Ile60 via alkyl interaction along with Tyr22 and Tyr58 via π-alkyl interactions. In addition, both pyrazine and benzene cores formed π-cation interaction with Arg54* and Lys9*, respectively. The remaining interactions were with Ala74, Ala75, Gly73, Asn72, Val56, Tyr90*, and Thr45* residues.

In contrast to **5d** (Fig. 4B), **5g** formed hydrogen bonds with Tyr90* and Thr57 residues rather than key residue Arg54*. It only interacted with the key residue Arg54* through π-cation interaction. The Cl atom and the pyrazine core of **5g** interacted with Val47* and Ile88* residues via both π-σ and alkyl interactions. In addition, the Cl atom interacted with Thr45* via a halogen interaction, which is a C-X interaction with structural properties akin to a weak hydrogen bond (Balasubramaniyan *et al*., 2018). Meanwhile, the cycloheptyl moiety of **5g** only formed an alkyl interaction with Ile86. The van der Waals interactions were observed between **5g** Tyr58, Pyr25, Gly73, Asn72, Val56, Ile60, Tyr22, Lys9*, His11*, and Ile46* residues.

Table 3. The binding energies and interacting residues of the pyrazinamides **5a–h**.

Pyrazinamide	Binding energy (kcal/mol)	Interacting residues				
		H-bonding	Hydrophobic interaction	Electrostatic interaction	Van der Waals	Halogen
5a	-5.92	-	π-σ: Ile88* π-alkyl: Val47*, Ile86*, Tyr90* alkyl: Val47*	Arg54*, Lys9*	Ala74, Tyr58, Thr57, Pyr25, Gly73, Asn72, Val56, Thr45*, Ile60, Tyr22	-
5b	-6.74	Thr57	π-σ: Val47* π-alkyl: Ile88*, His11* alkyl: Ile86*	Arg54*	Tyr58, Pyr25, Lys9*, Tyr90*, Gly73, Asn72, Thr45*, Ile60, Tyr22	-
5c	-5.50	Ala75, Arg54*	π-alkyl: Ile88*, Val47*, Tyr58 alkyl: Ile86*	Arg54*	Ala74, Ala75, Thr57, Pyr25, Lys9*, Tyr90*, Gly73, Asn72, Val56, Ile49*, His11*, Thr45*, Ile60, Tyr22	-
5d	-6.36	Arg54*	π-σ: Ile88*, Ile86*, Pyr25 π-alkyl: Val47*, Tyr58, Tyr22 alkyl: Ile60 π- π T-shaped: His11*	Arg54*, Lys9*	Ala74, Ala75, Tyr90*, Gly73, Asn72, Val56, Thr45*	-
5e	-2.83	Lys9*	π-σ: Pyr25 π-alkyl: Ile86*, Tyr58, Tyr90* alkyl: Ile88*, Val47*	-	Ala74, Ala75, Arg54*, Thr57, Gly73, Asn72, Val56, Ile49*, His11*, Thr45*, Tyr22	-
5f	-5.21	-	π-alkyl: Ile88*, Val47*, Ile86*, Tyr58, Tyr90*, Tyr22 alkyl: Val47*, Val56, Ile60	Arg54*, Lys9*	Ala74, Ala75, Thr57, Pyr25, Gly73, Asn72, Ile49*, His11*, Thr45*	-
5g	-5.91	Thr57, Tyr90*	π-σ: Ile88*, Val47* alkyl: Ile88*, Val47*, Ile86*	Arg54*	Tyr58, Pyr25, Lys9*, Gly73, Asn72, Val56, His11*, Ile60, Tyr22, Ile46*	Thr45*
5h	-5.51	Ala75, Arg54*	π-σ: Ile88* π-alkyl: Val47*, Tyr58, Tyr90*, Tyr22 alkyl: Ala74, Val47*, Ile86*, Ile60	-	Thr57, Pyr25, Lys9*, Gly73, Asn72, Val56, His11*, Thr45*	-
PZA	-5.21	Ala74, Asn72	π-σ: Pyr25 π-alkyl: Ile88*, Val47*, Ile86*	-	Ala75, Arg54*, Tyr58, Lys9*, Gly73, Ile49*, Ala76	-
NMJ (redocked)	-5.83	Ala74, Ala75, Arg54*	π-σ: Pyr25 π-alkyl: Ile88*, Val47*, Ile86* alkyl: Ile88*	Arg54*	Tyr58, Thr57, Lys9*, Tyr90*, Asn72, Gly73, Val56, Ile49*	-

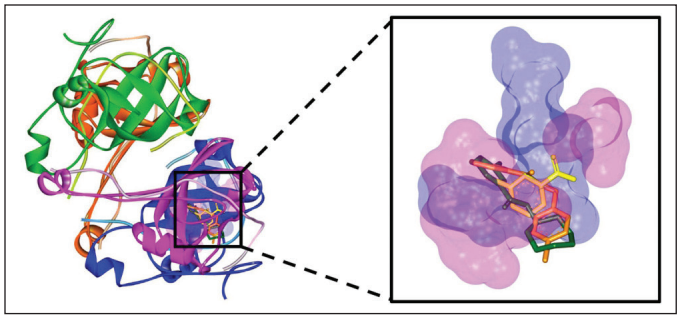

Figure 3. The binding conformations of **5d** (orange), **5g** (dark green), and NMJ (yellow) in the active site of *Mtb*PanD at the interface of subunits 1 (magenta) and 2 (blue) (PDB ID: 6P02).

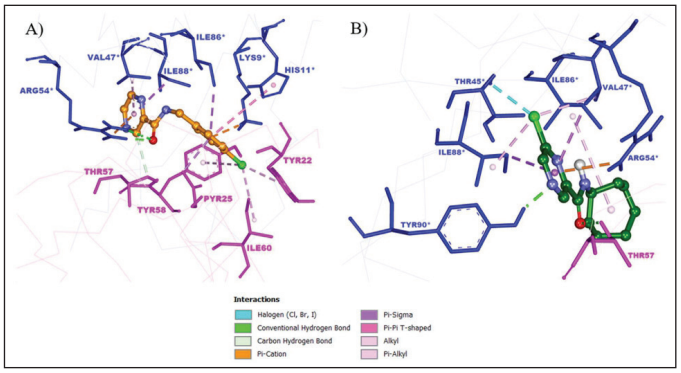

Figure 4. The binding mode of (A) **5d** and (B) **5g** at the active site of *Mtb*PanD between subunits 1 and 2 (PDB ID: 6P02). Subunit 1 residues are displayed in magenta, while subunit 2 residues are shown in blue.

CONCLUSION

Eight pyrazinamide analogs **5a–h** have been successfully synthesized by the Yamaguchi esterification method in up to 86% yield. Pyrazinamides **5d**, **g** exhibited the best antitubercular activity with a MIC value of <6.25 µg/ml. The molecular docking experiments using pyrazinamides **5a–h** at the active site of the *Mtb*PanD protein (PDB ID: 6P02), POA (PZA-activated form) targeted protein, revealed the probable binding interactions at the *Mtb*PanD active site. The docking results showed that **5d** and **5g** had lower binding energy than the 6P02 native ligand and pyrazinamide. These compounds are regarded as promising candidates for further optimization as antituberculosis drugs.

AUTHOR CONTRIBUTIONS

All authors made substantial contributions to the conception and design, acquisition of data, or analysis and interpretation of data; took part in drafting the article or revising it critically for important intellectual content; agreed to submit to the current journal; gave final approval of the version to be published; and agreed to be accountable for all aspects of the work. All the authors are eligible to be an author as per the international committee of medical journal editors (ICMJE) requirements/guidelines.

ACKNOWLEDGEMENTS

The authors would like to thank the Institut Teknologi Sepuluh Nopember for the WCP-like fund.

CONFLICTS OF INTEREST

The authors report no financial or any other conflicts of interest in this work.

ETHICAL APPROVALS

This study does not involve experiments on animals or human subjects.

DATA AVAILABILITY

All data generated and analyzed are included in this research article.

PUBLISHER'S NOTE

This journal remains neutral with regard to jurisdictional claims in published institutional affiliation.

REFERENCES

Abdel-Aziz M, Abdel-Rahman HM. Synthesis and anti-mycobacterial evaluation of some pyrazine-2-carboxylic acid hydrazide derivatives. Eur J Med Chem, 2010; 45(8):3384–8.

Adigun R, Singh R. Tuberculosis. StatPearls, StatPearls Publishing, Treasure Island, FL, 2022..

Alexander PE, De P. The emergence of extensively drug-resistant tuberculosis (TB): TB/HIV coinfection, multidrug-resistant TB and the resulting public health threat from extensively drug-resistant TB, globally and in Canada. Can J Infect Dis Med Microbiol, 2007; 18(5):289–91.

Annuur RM, Titisari DA, Dinarlita RR, Fadlan A, Ersam T, Nuryastuti T, Santoso M. Synthesis and anti-tuberculosis activity of trisindolines. AIP Conf Proc, 2018; 2049(1):020088.

Balasubramaniyan S, Irfan N, Umamaheswari A, Puratchikody A. Design and virtual screening of novel fluoroquinolone analogs as effective mutant DNA GyrA inhibitors against urinary tract infection-causing fluoroquinolone resistant *Escherichia coli*. RSC Advances 2018; 8(42):23629–47.

Bhargava A, Bhargava M. Tuberculosis deaths are predictable and preventable: comprehensive assessment and clinical care is the key. J Clin Tuberc Other Mycobact Dis, 2020; 19:100155.

Boechat N, Ferreira VF, Ferreira SB, de Lourdes G Ferreira M, de C da Silva F, Bastos MM, Dos S Costa M, Lourenço MCS, Pinto AC, Krettli AU, Aguiar AC, Teixeira BM, da Silva NV, Martins PRC, Bezerra FAFM, Camilo ALS, da Silva GP, Costa CCP. Novel 1,2,3-triazole derivatives for use against *Mycobacterium tuberculosis* H_{37}Rv (ATCC 27294) strain. J Med Chem, 2011; 54(17):5988–99

Bouz G, Semelková L, Janďourek O, Konečná K, Paterová P, Navrátilová L, Kubíček V, Kuneš J, Doležal M, Zitko J. Derivatives of 3-aminopyrazine-2-carboxamides: synthesis, antimicrobial evaluation, and *in vitro* cytotoxicity. Molecules, 2019; 24(7):1212.

Butman HS, Kotzé TJ, Dowd CS, Strauss E. Vitamin in the crosshairs: targeting pantothenate and coenzyme a biosynthesis for new antituberculosis agents. Front Cell Infect Microbiol, 2020; 10:605662.

Calnan M, Moran A, Jassim AlMossawi H. Maintaining essential tuberculosis services during the COVID-19 pandemic, Philippines. Bull World Health Organ, 2022; 100(2):127–34.

Dhimitruka I, SantaLucia J. Investigation of the yamaguchi esterification mechanism. Synthesis of a Lux-S enzyme inhibitor using an improved esterification method. Org Lett, 2006; 8(1):47–50.

Campanerut PAZ, Ghiraldi LD, Spositto FLE, Sato DN, Leite CQF, Hirata MH, Hirata RDC, Cardoso RF. Rapid detection of resistance to pyrazinamide in *Mycobacterium tuberculosis* using the resazurin microtitre assay. J Antimicrob Chemother, 2011; 66(5):1044–6.

Doležal M, Cmedlova P, Palek L, Vinsova J, Kuneš J, Buchta V, Jampilek J, Kráľová K. Synthesis and antimycobacterial evaluation of substituted pyrazinecarboxamides. Eur J Med Chem, 2008; 43(5):1105–13.

Doležal M, Zitko J, Kesetovicová D, Kuneš J, Svobodová M. Substituted *N*-phenylpyrazine-2-carboxamides: Synthesis and antimycobacterial evaluation. Molecules, 2009; 14(10):4180–9.

Evans JC, Trujillo C, Wang Z, Eoh H, Ehrt S, Schnappinger D, Boshoff HIM, Rhee KY, Barry CE, Mizrahi V. Validation of CoaBC as a bactericidal target in the coenzyme a pathway of *Mycobacterium tuberculosis*. ACS Infect Dis, 2016; 2(12):958–968.

Gentile D, Patamia V, Scala A, Sciortino MT, Piperno A, Rescifina A. Putative inhibitors of SARS-CoV-2 main protease from a library of marine natural products: a virtual screening and molecular modeling study. Mar Drugs, 2020; 18(4):225.

Gopal P, Sarathy JP, Yee M, Ragunathan P, Shin J, Bhushan S, Zhu J, Akopian T, Kandror O, Lim TK, Gengenbacher M, Lin Q, Rubin EJ, Grüber G, Dick T. Pyrazinamide triggers degradation of its target aspartate decarboxylase. Nat Commun, 2020; 11(1):1661.

Harini K, Jayashree S, Tiwari V, Vishwanath S, Sowdhamini R. Ligand docking methods to recognize allosteric inhibitors for G-protein-coupled receptors. Bioinform Biol Insights, 2021; 15:117793222110377.

Hassan NW, Saudi MN, Abdel-Ghany YS, Ismail A, Elzahhar PA, Sriram D, Nassra R, Abdel-Aziz MM, El-Hwash SA. Novel pyrazine based anti-tubercular agents: design, synthesis, biological evaluation and *in silico* studies. Bioorg Chem, 2020; 96:103610.

Bronowska AK. Thermodynamics of ligand-protein interactions: Implications for molecular design. In: Moreno Pirajn JC, (ed.). Thermodynamics - interaction studies - Solids, Liquids and Gases InTech, London, pp 1–48, 2011.

Kamadatu L, Santoso M. Synthesis and cytotoxicity of 4-allyl-2 methoxyphenol derivatives. IPTEK J Proc Ser, 2016; 2(1):193–4.

Kuitunen M-L, Cecilia Altamirano J, Siegenthaler P, Hannele Taure T, Antero Häkkinen V, Sinikka Vanninen P. Derivatization and rapid GC-MS screening of chlorides relevant to the chemical weapons convention in organic liquid samples. Anal Methods, 2020; 12(19):2527–35.

Maharani N, Santoso M. Synthesis of 2-phenylethyl esters by one-pot the yamaguchi esterification. Adv Environ Biol, 2015; 9(23):214–8.

Morris GM, Huey R, Lindstrom W, Sanner MF, Belew RK, Goodsell DS, Olson AJ. AutoDock4 and AutoDockTools4: automated docking with selective receptor flexibility. J Comput Chem, 2009; 30(16):2785–91.

Onajole OK, Pieroni M, Tipparaju SK, Lun S, Stec J, Chen G, Gunosewoyo H, Guo H, Ammerman NC, Bishai WRR, Kozikowski AP. Preliminary structure-activity relationships and biological evaluation of novel antitubercular indolecarboxamide derivatives against drug-susceptible and drug-resistant *Mycobacterium tuberculosis* strains. J Med Chem, 2013; 56(10):4093–103.

Pieroni M, Tipparaju SK, Lun S, Song Y, Sturm AW, Bishai WR, Kozikowski AP. Pyrido[1,2-a]benzimidazole-based agents active against tuberculosis (TB), multidrug-resistant (MDR) TB and extensively drug-resistant (XDR) TB. ChemMedChem, 2011; 6(2):334–42.

Santoso M, Ong LL, Aijijiyah NP, Wati FA, Azminah A, Annuur RM, Fadlan A, Judeh ZMA. Synthesis, α-glucosidase inhibition, α-amylase inhibition, and molecular docking studies of 3,3-di(indolyl)indolin-2-ones. Heliyon, 2022; 8:e09045.

Selvina. New paradigm of COVID-19 with pulmonary tuberculosis: a brief review. Eur J Med Health Sci, 2020; 2(6).

Semelkova L, Konecna K, Paterova P, Kubíček V, Kunes J, Novakova L, Marek J, Naesens L, Peško M, Kráľová K, Doležal M, Zitko J. Synthesis and biological evaluation of *N*-alkyl-3-(alkylamino)-pyrazine-2-carboxamides. Molecules, 2015; 20(5):8687–711.

Servusová B, Eibinová D, Doležal M, Kubíček V, Paterová P, Peško M, Kráľová K. Substituted *N*-benzylpyrazine-2-carboxamides: Synthesis and biological evaluation. Molecules, 2012; 17(11):13183–98.

Seung KJ, Keshavjee S, Rich ML. Multidrug-resistant tuberculosis and extensively drug-resistant tuberculosis. Cold Spring Harb Perspect Med, 2015; 5(9):a017863.

Sotgiu G, Centis R, D'ambrosio L, Migliori GB. Tuberculosis treatment and drug regimens. Cold Spring Harb Perspect Med, 2015; 5(5):a017822.

Sun Q, Li X, Perez LM, Shi W, Zhang Y, Sacchettini JC. The molecular basis of pyrazinamide activity on *Mycobacterium tuberculosis* PanD. Nat Commun, 2020; 11(1):339.

Tallei TE, Tumilaar SG, Lombogia LT, Adam AA, Sakib SA, Emran TB, Idroes R. Potential of betacyanin as inhibitor of SARS-CoV-2 revealed by molecular docking study. IOP Conf Ser: Earth Environ Sci, 2021; 711(1):012028.

Tamuzi JL, Ayele BT, Shumba CS, Adetokunboh OO, Uwimana-Nicol J, Haile ZT, Inugu J, Nyasulu PS. Implications of COVID-19 in high burden countries for HIV/TB: a systematic review of evidence. BMC Infect Dis, 2020; 20(1):744.

Teixeira C, Ventura C, Gomes JRB, Gomes P, Martins F. Cinnamic derivatives as antitubercular agents: Characterization by quantitative structure–activity relationship studies. Molecules, 2020; 25(3):456.

Wirth DD. Thionyl chloride. In: Encyclopedia of reagents for organic synthesis. John Wiley & Sons Ltd, New York, NY, 2001.

Yadav S, Pandey SK, Singh VK, Goel Y, Kumar A, Singh SM. Molecular docking studies of 3-bromopyruvate and its derivatives to metabolic regulatory enzymes: implication in designing of novel anticancer therapeutic strategies. PLoS One, 2017; 12(5):e0176403.

Zhang Y. Persistent and dormant tubercle bacilli and latent tuberculosis. Front Biosci, 2004; 9:1136–56.

Zhang Y, Wade MM, Scorpio A, Zhang H, Sun Z. Mode of action of pyrazinamide: disruption of *Mycobacterium tuberculosis* membrane transport and energetics by pyrazinoic acid. J Antimicrob Chemother, 2003; 52(5):790–5.

Zitko J, Barbora S-V, Paterová P, Navrátilová L, Trejtnar F, Kuneš J, Doležal M. Design, synthesis and anti-mycobacterial evaluation of some new *N*-phenylpyrazine-2-carboxamides. Chem Pap, 2016; 70(5):649–57.

Zitko J, Servusová B, Paterová P, Mandíková J, Kubíček V, Kučera R, Hrabcová V, Kuneš J, Soukup O, Doležal M. Synthesis, antimycobacterial activity and *in vitro* cytotoxicity of 5-chloro-*N*-phenylpyrazine-2-carboxamides. Molecules, 2013; 18(12):14807–25.

How to cite this article:
Zulqurnain M, Aijijiyah NP, Wati FA, Fadlan A, Azminah A, Santoso M. Synthesis, *Mycobacterium tuberculosis* H37Rv inhibitory activity, and molecular docking study of pyrazinamide analogs. J Appl Pharm Sci, 2023; 13(11):170–177.